Cement and Concrete Research 40 (2010) 370–375

Contents lists available at ScienceDirect

Cement and Concrete Research

journal homepage: http://ees.elsevier.com/CEMCON/default.asp

A comparative structural study of wet and dried ettringite

G. Renaudin [a,b], Y. Filinchuk [c], J. Neubauer [d], F. Goetz-Neunhoeffer [d,*]

[a] Clermont Université, ENSCCF, Laboratoire des Matériaux Inorganiques, BP 10448, F-63000 Clermont-Ferrand, France
[b] CNRS, UMR 6002, LMI, F-63177 Aubière, France
[c] Swiss–Norwegian Beam Lines at ESRF, 6 rue Jules Horowitz, BP 220, 38043 Grenoble, France
[d] University of Erlangen, GeoZentrum Nordbayern, Mineralogy, Schlossgarten 5 a, 91054 Erlangen, Germany

ARTICLE INFO

Article history:
Received 29 July 2008
Accepted 5 November 2009

Keywords:
Ettringite (D)
Crystal structure (B)
X-ray diffraction (B)
Raman spectroscopy (B)
Hydration (A)

ABSTRACT

Two different techniques were used to compare structural characteristics of "wet" ettringite (stored in the synthesis mother liquid) and "dried" ettringite (dried to 35% relative humidity over saturated $CaCl_2$ solution). Lattice parameters and the water content in the channel region of the structure (site occupancy factor of the water molecule not bonded to cations) as well as microstructure parameters (size and strain) were determined from a Rietveld refinement on synchrotron powder diffraction data. Local environment of sulphate anions and of the hydrogen bonding network was characterized by Raman spectroscopy. Both techniques led to the same conclusion: the "wet" ettringite sample immersed in the mother solution from the synthesis presents similar structural features as ettringite dried to 35% relative humidity. An increase of the *a* lattice parameter combined with a decrease of the *c* lattice parameter occurs on drying. The amount of structural water, the point symmetry of sulphate and the hydrogen bond network are unchanged when passing from the wet to the dried ettringite powder. Ettringite does not form a high-hydrate polymorph in equilibrium with alkaline solution, in contrast to the AFm phases that lose water molecules on drying. According to these results we conclude that ettringite precipitated in aqueous solution at the early hydration stages is of the same chemical composition as ettringite present in the hardening concrete.

1. Introduction

Ettringite, $Ca_6Al_2(OH)_{12}\cdot(SO_4)_3\cdot\sim 26H_2O$, is a mineral which rarely occurs in nature but is widely present in the mineralogy of hydrated cements: in the different types of Portland cement, in calcium aluminate cements in combination with calcium sulphates as well as in the calcium sulfoaluminate cement. In cement chemistry, ettringite is commonly named AFt, similar to the AFm phases of the general formula $Ca_4(Al,Fe)_2(OH)_{12}\cdot X_z\cdot nH_2O$ (where *X* is an anion). The formation of ettringite during the early hydration stage is important for controlling the rate of set of the highly reactive aluminate phases [1]. Nevertheless, its formation in mature cement stone can be destructive, such as the result of sulphate attack [2] or the formation of delayed ettringite [3]. This important mineral in cement chemistry has a beneficial effect at the early stage of hydration in extremely wet paste and might damage hardened concrete if formed in the cement stone after longer times. Ettringite has been the subject of numerous studies in the cement chemistry. Its structural description has been continuously improved from the first models reported before 1970 by Moore and Taylor [4,5] up to the other more recent crystallographic works [6,7]. The use of neutron [7] and high resolution [6] powder diffraction provided a full crystallographic description of ettringite, including a complete characterization of its hydrogen bonding network. Details of the structural description of ettringite were confirmed by Raman spectroscopic study [8]. Other efforts have been concentrated on the ettringite crystallization in wet cement paste during the early hydration period of up to 24 h [9,10]. Ettringite is the first and the only hydrate formed during the hydration of tricalcium aluminate in the presence of gypsum [11]. Lattice parameters of ettringites were evaluated during hydration of the cement pastes consisting of pure OPC (Ordinary Portland Cement). For all investigated cements an increase of the lattice parameter *a* was observed [9] during the first hours of hydration: it increases mostly during the induction period (Fig. 1) and reaches 11.212 Å after 19.1 h. The lattice parameter *c* of ettringites from pure cement paste is initially 21.610 Å immediately after contact with water. During the following induction and acceleration period the *c* lattice parameter strongly decreases down to 21.494 Å after 19.1 h. The evolution of structural changes during the thermal decomposition of dried ettringite (dried over saturated LiCl solution to 11% relative humidity) showed a large variation of the water amount (close to 18 water molecules per formula unit) before the transition to an amorphous state and occurring with a extremely weak variations of the lattice parameters (0.2% increase of the *a* lattice parameter and 0.4% decrease of the *c* lattice parameter) [12].

* Corresponding author. Present address: Schlossgarten 5a, D-91054 Erlangen, Germany. Tel.: +49 9131 8525780.
E-mail address: goetz@geol.uni-erlangen.de (F. Goetz-Neunhoeffer).

0008-8846/$ – see front matter © 2009 Elsevier Ltd. All rights reserved.
doi:10.1016/j.cemconres.2009.11.002

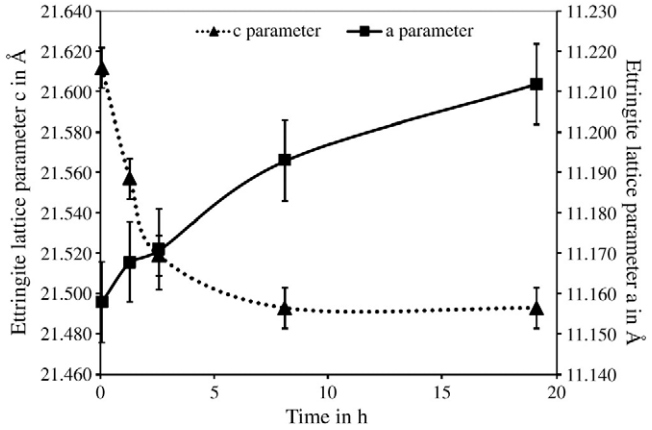

Fig. 1. Lattice parameters *a* and *c* of ettringites during early hydration of OPC paste [9]. Lattice parameter *a* increases from 11.159 to 11.212 ± 0.01 Å and lattice parameter *c* strongly decreases from 21.61 Å down to 21.49 ± 0.01 Å.

No structural study was performed on ettringite kept in its mother alkaline synthesis solution in order to verify the existence of a highly hydrated form. Such a kind of water-rich form in alkaline aqueous suspension is well known in the case of the AFm phases [1,13–15]. Our study aimed to compare the crystallographic feature of the wet ettringite (*i.e.* keep in the solution which corresponds to the conditions of its formation at the early stage of hydration) with the dried ettringite (corresponds to the condition in a hardened cement stone). Two ettringite samples were synthesised: one was kept in the synthesis solution and the other was filtered off and dried. Both samples were analyzed by Rietveld refinement on synchrotron powder diffraction patterns and Raman spectroscopy in order to combine characterizations of the long range order and of the local environment. The samples were then compared in terms of varied structural parameters (namely lattice parameters and structural water content), local environment of sulphate anions and hydrogen bonding network.

2. Experimental

2.1. Syntheses

In order to permit high concentration of CaO while inhibiting precipitation of $Ca(OH)_2$, the CaO was dissolved in aqueous solutions of sucrose as described initially by Carlson and Berman [16]. To prevent contamination by atmospheric CO_2 all preparative work was performed in N_2 atmosphere. Ettringite was prepared from sucrose/CaO-suspension (68 mmol CaO/L and 292 mmol sucrose/L). Al^{3+} and SO_4^{2-} were supplied from an aqueous CO_2-free solution of $Al_2(SO_4)_3 \cdot nH_2O$ with concentration of 11.4 mmol/L. In order to precipitate ettringite crystals the two reaction solutions were mixed with CaO to Al_2O_3 molar ratio of 6:1. Synthesis experiments were performed at a constant temperature of 23 ± 0.5 °C. After 2 days the precipitates were filtered off the synthesis solution and washed with aqueous ammonia (pH 12) to prevent partial dissolution of ettringite at neutral pH [17] and to ensure the complete removal of synthesis solution. The wet as-synthesized ettringite sample was stored for the following investigations. The dried ettringite sample was dried over a saturated $CaCl_2$ solution (35% relative humidity) to equilibrium condition. For the X-ray analysis, the dried ettringite powder was gently ground with an agate mortar.

2.2. Powder X-rays diffraction measurements (PXRD)

Synchrotron powder diffraction data were obtained for both samples at Swiss–Norwegian Beam Lines at ESRF (Grenoble, France). The samples were introduced into 0.5 mm diameter glass capillaries. The wet ettringite sample was introduced as a wet paste composed by the ettringite powder immersed in its mother alkaline solution. Data collections were performed at 295 K with a MAR345 Image Plate detector by using a monochromatic wavelength of λ = 0.722420 Å. The calculated absorption coefficient $m\mu R$ (m = powder packing factor, μ = linear absorption coefficient, R = radius of the capillary) was estimated as 0.80. Repetitive measurements showed the non-destructive nature of the X-ray dose. Two sample-to-detector distances were used (150 and 250 mm) in order to combine the advantages of high structural and angular resolutions. The detector parameters and the wavelength were calibrated with NIST LaB_6. The highest resolution of the MAR345 detector was used: 3450 × 3450 pixels with a pixel size of 100 μm. During the 60 s exposure time the capillaries were rotated by 60°. The two-dimensional (2D) data were integrated with *Fit2D* program [18]. Very high counting statistics, exceeding 10^7 counts per step in 2θ permits precise definition of the background line and observation of very weak diffraction peaks. Highly accurate integrated intensities were obtained from a good powder average achieved by projecting the whole scattering information on the 2D detector. Uncertainties of the integrated intensities were calculated at each 2θ-point applying Poisson statistics to the intensity data, considering the geometry of the detector [19]. The instrument resolution functions were determined from the LaB_6 data. In the case of the wet ettringite sample, patterns were measured twice in order to verify an absence of the reaction between the alkaline solution and the glass capillary.

2.3. Raman spectroscopy

The employed Raman instrument was a Renishaw inVia spectrometer, specially adapted at SNBL for remote measurements. Spectra were recorded on the same capillaries as used in PXRD measurements: one with the dried ettringite sample, another with the wet ettringite in the presence of alkaline solution, and in addition on one capillary filled only with the alkaline solution extracted at the end of the ettringite synthesis. The green 535 nm laser and 1800 lines/mm grating were used. The spectral resolution was about 2 cm^{-1}. The laser beam with a total power of 75 mW was focused onto the sample with 250 μm focal spot; the large focal spot helped to avoid any damage to the material, spectra obtained at different power load were identical. The grating calibration was controlled by checking the position of the Raman line of a Si standard at 520 cm^{-1}. The Raman spectra were collected using a time accumulation 20 s per scan, and merging five consecutive scans. Spectra were analyzed by using the profile fitting procedure with a Lorentzian function of the program *SPECTRAW* [20]. Spectra were recorded in the frequency ranges 100 cm^{-1}–1200 cm^{-1} and 3000 cm^{-1}–4000 cm^{-1} in order to investigate the four Raman active vibration modes of sulphate anions, the 'Al$(OH)_6$' octahedron vibration and the hydrogen bond network due to the water and hydroxyl stretching. Spectra have also been recorded on the mother alkaline solution in order to subtract its signal from the spectra recorded on the wet sample.

2.4. Rietveld refinements

Joint Rietveld refinements based on the simultaneous use of the data measured at 150 mm (large 2θ interval) and 250 mm (high resolution) sample-to-detector distances were performed for dried and wet samples with the program *Fullprof.2k Multi-Pattern* [21]. The dried and wet ettringites were proved to be single phase samples. The structural parameters of ettringite, $Ca_6Al_2(OH)_{12} \cdot (SO_4)_3 \cdot \sim 26H_2O$, were taken from Goetz-Neunhoeffer and Neubauer [6] (a revised structure model proposed by Moore and Taylor [4,5], supplemented by the H positions determined by Hartman and Berliner [7]): space group $P31c$, $Z = 2$, $a = 11.229$ Å and $c = 21.478$ Å, 48 independent atomic positions: 2 Al (special site 2*a*, with *z* coordinates fixed at 0 and 1/4 for respectively Al1 and Al2 sites), 2 Ca (general position 6*c*),

three S (special position 2*b*), 19 O (four hydroxyl anions on general position 6*c*, nine water molecules on general position 6*c* and six oxygen atoms from sulphate groups distributed on general 6*c* and special 2*b* positions), 22 H (general position 6*c* from four hydroxyl anions and nine water molecules). The channel water molecule, described by the atomic positions O19, H19a and H19b according to atomic labels used in [5–7], has a partial occupancy factor. The determination of the Instrumental Resolution Functions (extracted from the powder patterns recorded on NIST LaB_6 powder) allowed the extraction of the sample intrinsic microstructure parameters: average apparent crystallite size and average maximum strain. The diffraction profiles (both instrumental and sample intrinsic) were modelled by using a Thomson–Cox–Hastings pseudo-Voigt function [21]. Joint Rietveld refinements were performed with lattice parameters, peak profile parameters and anisotropic microstructure parameters constrained to be equivalent for the data recorded at 150 and 250 mm. The zero shifts, preferred orientations and asymmetry parameters were not constrained. Six isotropic temperature factors, B_{iso}, were refined: for Al, Ca, S atoms, and for O from hydroxyl groups, water molecules and sulphate anions. Hydrogen atoms were included in the refinement and their isotropic temperature factors were constrained to be 1.2 times B_{iso} of the corresponding oxygen atom, in accordance with previously published data from related AFm phases [22–24]. Fractional coordinates of the 48 independent positions were fixed at the values indicated by Goetz-Neunhoeffer and Neubauer [6]. In the final run the occupancy parameter of the channel water molecule was let to vary freely, leading to stable refinements of 32 parameters (2 scale factors, 2 zero shifts, 2 lattice parameters, 3 peak profile parameters, 7 anisotropic size model parameters, 3 anisotropic strain model parameters, 2 preferred orientation parameters, 4 asymmetry parameters, 6 isotropic temperature factors and 1 occupancy factor). Care has been taken during the last cycles of refinement on the weak correlation between the refined parameters related to the average apparent domains size and the internal strains. Any increase of Full Width at Half maximum (FWHM) in the observed diffraction profile with respect to the instrumental FWHM was considered to be intrinsic to the sample. Anisotropic average crystallite size and anisotropic strain effects were then separated and refined from the deconvolution in two Lorentzian and Gaussian components of the intrinsic line broadening and due to their distinct angular dependences. The refined structure and microstructure parameters are summarized in Table 1 and the joint Rietveld plots of dried and wet ettringite samples are respectively shown in Figs. 2 and 3.

Table 1
Structure and microstructure parameters refined by joint Rietveld analyses on dried and wet ettringite samples.

		Dry ettringite	Wet ettringite
Structure parameters (standard uncertainties in parentheses)			
a (Å)		11.2220 (3)	11.2129 (3)
c (Å)		21.4327 (5)	21.4783 (5)
V (Å^3)		2337.5 (1)	2338.7(1)
Channel water occupancy		0.83 (2)	0.80 (2)
B_{iso} (Å^2) – Al		0.8 (1)	1.0 (2)
– Ca		1.13 (5)	0.83 (5)
– OH	$B_{iso}(Oh)$[a]	0.8 (1)	0.4(1)
	$B_{iso}(Hh)$[a]	0.9 (–)	0.5 (–)
– H_2O	$B_{iso}(Ow)$[a]	2.4 (1)	2.0 (1)
	$B_{iso}(Hw)$[a]	2.9 (–)	2.4 (–)
– SO_4	$B_{iso}(S)$	1.8 (1)	1.6 (1)
	$B_{iso}(Os)$[a]	4.6 (2)	4.4 (2)
Microstructure parameters (mean anisotropy in parentheses)			
Average apparent size (Å)		600 (120)	820 (130)
Size along [002] (Å)		250	420
Size along [100] (Å)		600	780
Size along [102] (Å)		675	900
Average maximum strain (‰)		2.0 (0.3)	1.6 (0.1)
Strain along [002] (‰)		0.9	1.8
Strain along [100] (‰)		1.6	1.7
Strain along [102] (‰)		2.4	1.4
Reliability Rietveld factors for patterns recorded at 150 and 250 mm respectively			
R_{Bragg}		0.036, 0.032	0.047, 0.035
R_f		0.032, 0.035	0.043, 0.033
R_p		0.071, 0.065	0.078, 0.070
R_{wp}		0.068, 0.064	0.077, 0.072

[a] Label *h*, *w* and *s* refer respectively to atoms from hydroxyl anions, water molecules and sulphate groups.

3. Results and discussion

3.1. Synchrotron powder X-ray diffraction

Synchrotron powder diffraction patterns for the wet ettringite sample are similar to those for the dried ettringite sample (Figs. 2 and 3). The main difference concerns the broad scattering signal superposed on the background at 2θ around 10°, which arises predominantly from the vitreous glass capillaries. The broad scattering signal, observed for both ettringite samples, is more pronounced in the case of the dried one. The difference observed for the intensity of this amorphous scattering signal comes from the thickness of the capillary and the powder packing efficiency (*i.e.* the mass ratio between the amorphous glass and the introduced crystalline powder). The diffraction signal of the wet ettringite sample is similar to that of the dried ettringite sample indicating that the well-known structure of dried ettringite [4–7] is preserved when crystals of ettringite are kept suspended in the mother alkaline solution. There is apparently no modification of the symmetry class, no symmetry lowering and no appearance of superstructure diffraction peaks. Nevertheless a small, but significant, variation of the lattice parameters is observed (see Table 1). The variations of the *a* and *c* lattice parameters are of the opposite sign, leading to a very small decrease of the unit cell volume when drying. The *a* lattice parameter increases from 11.2129(3) Å to 11.2220(3) Å and the parameter *c* decreases from 21.4783(5) Å to 21.4327(5) Å after drying of the wet ettringite to 35% relative humidity over saturated $CaCl_2$ solution. The same variations have been observed during the dehydration process (weak increase of the lattice parameter *a*, and weak decrease of the lattice parameter *c*) [12]. Thus, the drying of ettringite leads to 0.08% increase of *a* and 0.21% decrease of *c*; this corresponds to a small −0.05% decrease of the unit cell volume. A comparison with the unit cell parameters of the ettringite samples measured during its nucleation and growth in solution [10] indicates a continuous decrease of the *c* lattice parameter when precipitating (from 22.00 Å to 21.48 Å: [10]) and drying (from 21.48 Å to 21.43 Å: this study). In the case of the *a* lattice parameter a continuous increase is observed when precipitating (from 11.08 Å to 11.24 Å: [10]) and drying (from 11.21 Å to 11.22 Å: this study). The unit cell variations are not accompanied with a modification of the amount of structural water in ettringite although this was observed when dried ettringite samples (11% relative humidity) were investigated at 50 °C under a flow of dry nitrogen [12]. Dried ettringite is then changing lattice parameter in dependence of relative humidity accompanied by reduction of occupancy of A-water, B-water, hydroxyl O and channel water sites (labels A and B are taken from [12]). However the investigated wet (100% relative humidity) and dried (35% relative humidity) ettringite samples from our synthesis showed no change of chemical water content according to the refined occupancies of the channel water site before and after drying. As indicated in Table 1, the occupancy factor of the channel water molecule site is not affected by drying. An insignificant increase from 0.80(2) to 0.83(2) is observed when going from the wet to the dried ettringite, leading to the following refined compositions: $Ca_6Al_2(OH)_{12}\cdot(SO_4)_3\cdot 26.40(6)H_2O$ and $Ca_6Al_2(OH)_{12}\cdot(SO_4)_3\cdot 26.49(6)H_2O$ respectively for wet and dried ettringite. Our refined channel water site occupancies are higher than the previously published values (0.499 [7], 0.56 [5] and 0.667 [6]), nevertheless the commonly used notation $Ca_6Al_2(OH)_{12}\cdot(SO_4)_3\cdot\sim 26H_2O$ for the ettringite composition is still acceptable

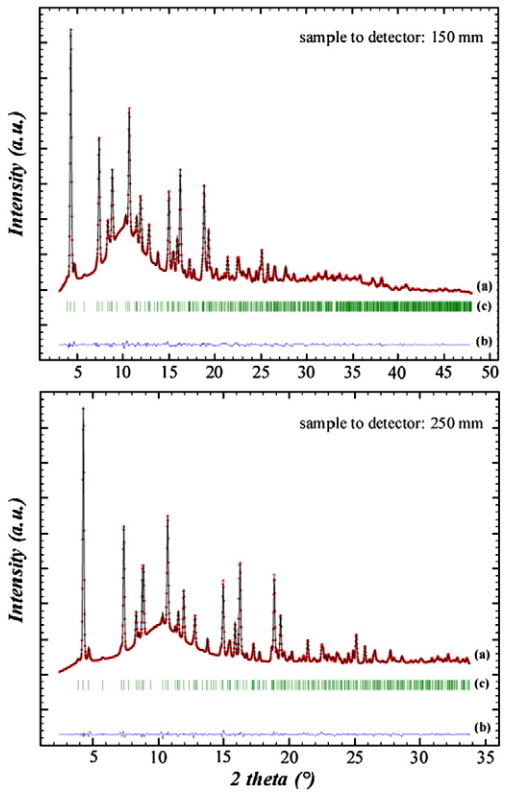

Fig. 2. Powder patterns from the joint Rietveld refinement on the dried ettringite sample. Two sample-to-detector distances represent the top (150 mm) and the bottom (250 mm) plots. The data were measured at SNBL, ESRF with MAR345 Image Plate detector and λ = 0.722420 Å. Observed (a: red dots), calculated (a: black curve) and difference (b: blue curve) patterns are represented with the Bragg peak positions of ettringite (c: green bars). (For interpretation of the references to colour in this figure legend, the reader is referred to the web version of this article.)

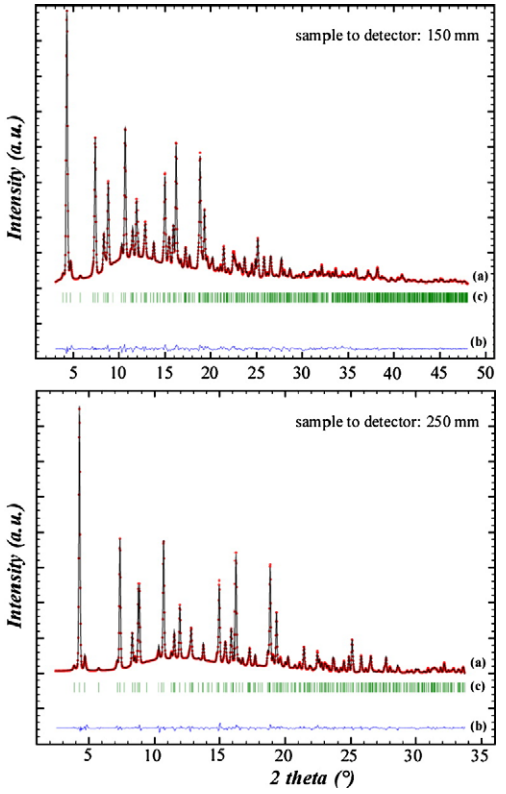

Fig. 3. Powder patterns from the joint Rietveld refinement on the wet ettringite sample. Two sample-to-detector distances represent the top (150 mm) and the bottom (250 mm) plots. The data were measured at SNBL, ESRF with MAR345 Image Plate detector and λ = 0.722420 Å. Observed (a: red dots), calculated (a: black curve) and difference (b: blue curve) patterns are represented with the Bragg peak positions of ettringite (c: green bars). (For interpretation of the references to colour in this figure legend, the reader is referred to the web version of this article.)

$(Ca_6Al_2(OH)_{12}\cdot(SO_4)_3\cdot 25.5H_2O$, and $Ca_6Al_2(OH)_{12}\cdot(SO_4)_3\cdot 26.5H_2O$ respectively, for the channel site occupancy of 0.499 [7], and 0.83 respectively). Similar to the channel water site occupancy, the isotropic atomic displacement parameters of cations, anions and water molecules are close for both samples. Contrary to AFm phases, we could show with this comparative investigation of wet and dried sample that ettringite does not form a water-richer modification than $Ca_6Al_2(OH)_{12}\cdot(SO_4)_3\cdot\sim 26H_2O$ in contact with the synthesis solution. In the calcium aluminate AFm system, $Ca_4Al_2(OH)_{12}\cdot(OH)_2\cdot 12H_2O$ phase is stable in equilibrium with the alkaline solution, but it converts to the air-dried phase $Ca_4Al_2(OH)_{12}\cdot(OH)_2\cdot 6H_2O$ [1,13–15,25] with a loss of six water molecules. This transition is accompanied by a 0.5% decrease of the *a* and a large 25.8% decrease of the *c* lattice parameters (the unit cell volume decrease is about 26.6%). Monosulfoaluminate shows a similar behaviour: water content in the water-rich $Ca_4Al_2(OH)_{12}\cdot SO_4\cdot 8H_2O$ phase (stable in solution) decreases on drying to $Ca_4Al_2(OH)_{12}\cdot SO_4\cdot 6H_2O$ [26,27]. The drying of monosulfoaluminate is accomplished by 6.3% decrease of the unit cell volume, as does the nitrated AFm phase $Ca_4Al_2(OH)_{12}\cdot(NO_3)_2\cdot 4H_2O$ at around 50 °C during its partial dehydration (departure of two water molecules displaying a 7.0% unit cell volume decrease) [28,29]. The dehydrations of the high-hydrated AFm phases are always accompanied by a large decrease of the unit cell volume through the large decrease of the *c* lattice parameter. In our study of the AFt phase (wet and dried ettringite) such an unit cell evolution is not observed, in agreement with the constant refined amount of water in ettringite structure found before and after drying.

Refined microstructure parameters reveal changes upon the drying (see Table 1). Anisotropic average apparent shape of the coherent domains (plate-like hexagonal domains) does not correlate with the visible needle-shaped ettringite crystals (showed as microphotographs in [30]). Ettringite crystals, hexagonal prisms elongated along the [001] direction, are composed of several coherent hexagonal plate-like domains. Dried ettringite crystals reveal a more pronounced anisotropy and a decrease of the coherent domain size. Compared to the wet form, the size decreases by about 40% along the hexagonal *c* axis (along [002], Table 1) and only about 23% in the hexagonal plane (along [100], Table 1). At the same time, strains are considerably relaxed along the hexagonal axis (50% decrease). These observations can be interpreted by a presence of faults in the sulphate sequence along the *c* axis generated by the trigonal symmetry (see Fig. 5 from Goetz-Neunhoffer and Neubauer [6]: sulphate down–sulphate up–sulphate up–channel water– …). Numerous faults in the sulphate orientation sequence divide the visible needle-shaped crystal into several plate-like hexagonal domains along the *c* axis. On drying these coherent domains are broken, thus explaining the decrease of the average apparent domains size (from 820 Å to 600 Å) and the loss of the internal strains along the hexagonal *c* axis (from 1.8‰ to 0.9‰).

3.2. Raman spectroscopy

Raman spectroscopy can be a useful tool to compare the wet and the dried ettringite samples. Local environment of sulphate anions and hydrogen bonding network have been described using Raman spectroscopy in sulphated cement hydrates [8]. Raman spectroscopy has also been useful to follow the partial dehydration of the nitrated AFm phase [28,29]. Fig. 4 represents the Raman spectra recorded on the dried and the wet ettringite samples and on the alkaline solution extracted from the synthesis. Profile fitting of the spectra was performed and results are collected in Table 2 (band positions, widths and assignments). The four active modes of vibration of sulphate, as well as the $[Al(OH)_6]$ vibration are very similar (see the positions and

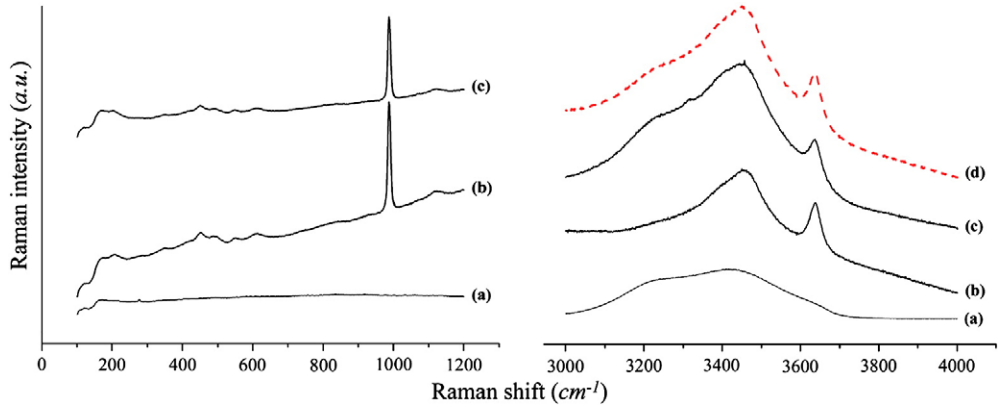

Fig. 4. Raman spectra recorded in the range 100–1200 cm^{-1} (left) and 3000–4000 cm^{-1} (right) on a: mother alkaline solution extracted from the synthesis, b: dried ettringite sample, and c: wet ettringite sample. The d curve is the combination of the a spectrum (alkaline solution) with the b spectrum (dried ettringite).

band widths in Table 2) in both dried and wet samples. This is a clear indication of the similar identical environment of sulphate anion in both samples (the same point symmetry and the same environment for the channel and bonded water molecules). No free solvated sulphate could be detected in the synthesis solution as indicated by the absence of a signal on the spectra recorded from the alkaline solution. The Raman spectra recorded in the 3000–4000 cm^{-1} range are used to investigate the hydrogen bond network: O–H elongation from hydroxyl anions and water molecules (structural bonded, structural free and liquid water). The Raman signal from the mother alkaline solution shows several extremely broad and unresolved bands. This signal of the liquid is present in the spectra recorded on the wet ettringite sample (as wet ettringite was kept immersed in its alkaline mother solution). Deconvolution of the spectra in the range 3000–4000 cm^{-1} from wet ettringite was not trivial due to the presence of broad bands with unresolved broad shoulders. Nevertheless results from deconvolution indicated in Table 2 show that there is no new band of vibration in the wet ettringite sample; *i.e.* we observe the bands from dried ettringite combining with the bands from the alkaline solution. The curve d in Fig. 4 is a combination of the spectra from the dried ettringite (curve b) with the spectra from the mother alkaline solution (curve a). This curve d superimposes remarkably well on the curve c recorded on the wet ettringite sample. This is a clear indication of the presence of the same hydrogen bonding network, represented in Fig. 5, both in dried and wet ettringites (*i.e.* the same bonded water and channel water molecules in both samples). As well as in dried ettringite, the intercolumn cohesion in wet ettringite is achieved by twelve hydrogen bonds around each sulphate group (bonded to twelve water molecules bonded to calcium atoms) and by four hydrogen bonds around each channel water molecules (bonded to four water molecules bonded to calcium atoms).

Table 2
Assignment and position (cm^{-1}) of the bands of vibration for the three samples (half widths at half maximum are indicated in parentheses, cm^{-1}).

	Dried ettringite	Wet ettringite	Alkaline solution
100 cm^{-1}–1200 cm^{-1} range			
	346.4 (14.7)	345.4 (14.0)	
	414.3 (25.7)	415.2 (22.2)	
ν_2 [SO_4]	452.1 (15.8)	451.6 (15.8)	
	492.1 (21.6)	492.6 (21.1)	
[$Al(OH)_6$]	548.7 (10.2)	547.9 (11.3)	
ν_4 [SO_4]	610.2 (22.2)	610.7 (21.5)	
ν_1 [SO_4]	988.5 (4.7)	988.4 (4.7)	
ν_3 [SO_4]	1120.0 (25.6)	1120.2 (25.1)	
3000 cm^{-1}–4000 cm^{-1} range			
[H_2O] stretching		3229.8 (119.2)	3228.3 (126.1)
[H_2O] stretching	3289.2 (199.4)^{sh}		
[H_2O] stretching		3312.5 (12.4)	3316.7 (31.3)^{sh}
[H_2O] stretching	3404.7 (75.6)^{sh}	3399.7 (124.7)^{sh}	
[H_2O] stretching		3416.8 (117.4)	3434.3 (183.5)
[H_2O] stretching	3464.2 (45.8)	3468.3 (67.3)	
[H_2O] stretching	3517.4 (107.8)^{sh}		
[OH] stretching			3620.5 (41.1)^{sh}
[OH] stretching	3638.0 (18.5)	3637.9 (20.9)	

^{sh}: shoulder.

4. Conclusion

The structure of ettringite, which was kept immersed in its mother alkaline synthesis solution, was investigated by a comparative study with an ettringite dried to 35% relative humidity over $CaCl_2$. Crystallographic study (based on Rietveld refinement using synchrotron powder diffraction data) and investigation of the local environment (based on Raman spectroscopy) indicate that the wet and dried ettringite structures are similar. Crystallographic characterization of wet ettringite showed a small evolution of lattice parameter (an increase of the *a* lattice parameter and a decrease of the *c* lattice parameter), which was not accompanied by any structural modification. The amount of channel water remains intact. The only difference concerns the microstructural parameters: the apparent crystallite size decreases on drying. The same results were obtained by Raman spectroscopy. Vibrational spectra recorded for the wet and dried ettringite samples show the same bands of vibration. The local environments of the sulphate anion and water molecules in wet ettringite closely resemble those in dried ettringite. Only during dehydrating already dried ettringite samples at 50 °C a simultaneous loss of water and hydroxyl molecules from the ettringite structure was determined, based upon direct measurement of the water and hydroxyl molecule occupancies from structural refinement of neutron diffraction data [12]. However the result of our study provides evidence that the same ettringite structure appears irrespective of the experimental conditions (wet and dry), in contrast to most of the AFm phases that lose water molecules on drying. According to these results we conclude that ettringite precipitated in aqueous solution at the early hydration stages is of the same chemical composition as ettringite formed during the hardening of concrete. The curing process of concrete at room temperature has no direct effect on the ettringite composition. Because the water occupancy factors of ettringite are independent of experimental conditions (wet and dry) the observed lattice parameter changes could not be related to the loss of H_2O.

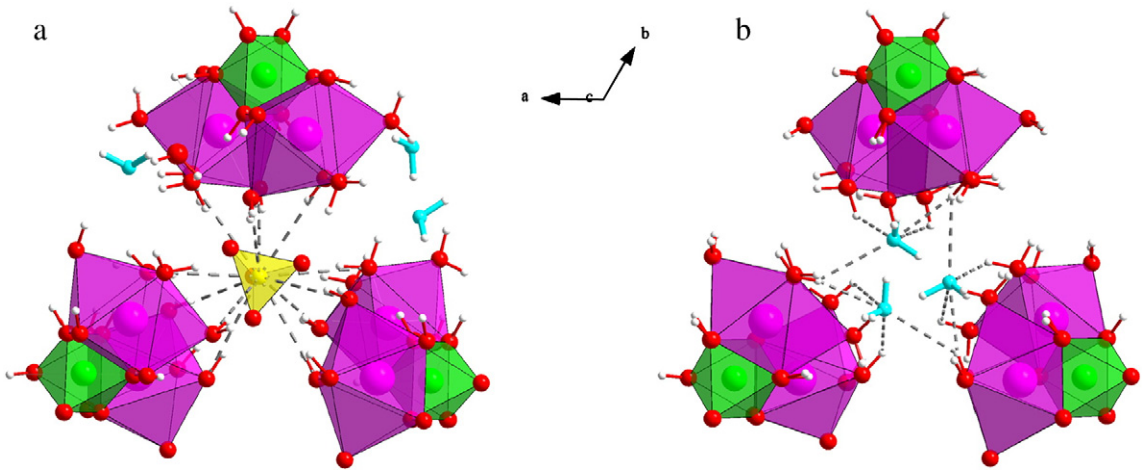

Fig. 5. Representation of the hydrogen bonding network (broken grey bonds) providing the intercolumn cohesion in the ettringite structure around sulphate anions (a) and channel water molecules (b). Green, pink and yellow polyhedra represent respectively six-fold coordinated aluminium atoms (by six hydroxyl groups), eight-fold coordinated calcium atoms (by four hydroxyl groups and four bonded water molecules) and sulphate anions. Hydroxyl groups and bonded water molecules are represented in red, channel water molecules are represented in blue (small white spheres represent hydrogen atoms). (For interpretation of the references to colour in this figure legend, the reader is referred to the web version of this article.)

Acknowledgements

The authors are grateful to SNBL for the in-house beam time allocation and Wouter van Beek for the help with the Raman experiment.

References

[1] H.F.W. Taylor, Cement Chemistry, 2nd ed., Thomas Telford, London, 1997.
[2] M. Santhanam, M.D. Cohen, J. Olek, Cem. Concr. Res. 31 (2001) 845.
[3] H.F.W. Taylor, C. Famy, K.L. Scrivener, Cem. Concr. Res. 31 (2001) 683.
[4] A.E. Moore, H.F.W. Taylor, Nature 218 (1968) 1048.
[5] A.E. Moore, H.F.W. Taylor, Acta Cryst. B26 (1970) 386.
[6] F. Goetz-Neunhoeffer, J. Neubauer, Powder Diffr. 21 (1) (2006) 4.
[7] M.R. Hartman, R. Berliner, Cem. Concr. Res. 36 (2006) 364.
[8] G. Renaudin, R. Segni, D. Mentel, J.-M. Nedelec, F. Leroux, C. Taviot-Gueho, J. Adv. Concr. Tech. 5 (2007) 299.
[9] J. Neubauer, F. Goetz-Neunhoeffer, U. Holland, D. Schmitt, P. Gaeberlein, M. Degenkolb, M., Crystal chemistry and microstructure of hydrated phases occurring during early OPC hydration, Proceedings of the 12th International Congress on the Chemistry of Cement (12th International Congress on the Chemistry of Cement Montréal 08-13.07.2007), 2007.
[10] M. Merlini, G. Artioli, T. Cerulli, F. Cella, A. Bravo, Cem. Concr. Res. 38 (2008) 477.
[11] M.R. Hartman, R. Berliner, J. Sol. State Chem. 178 (2005) 3256.
[12] M.R. Hartman, S.K. Brady, R. Berliner, M.S. Conradi, J. Sol. State Chem. 179 (2006) 1259.
[13] M.H. Roberts, J. Appl. Chem. 10 (1957) 543.
[14] E. Aruja, Acta Cryst. 13 (1960) 1018.
[15] E. Aruja, Acta Cryst. 14 (1961) 1213.
[16] E.T. Carlson, H.A. Berman, J. Res. NBS 64A (1960) 333–341.
[17] P. Kumarathasan, G.J. McCarthy, D.J. Hassett, D.F. Pflughoeft-Hassett, Oxyanion substituted ettringites: synthesis and characterization; and their potential role in immobilization of As, B, Cr, Se, and V, Fly Ash and Coal Conversion By-products: Characterization, Utilization, and Disposal VI, Materials Research Society Symposium Proceedings, vol. 178, 1990, pp. 83–104.
[18] A.P. Hammersley, S.O. Svensson, M. Hanfland, A.N. Fitch, D. Häusermann, High Pressure Res. 14 (1996) 235–248.
[19] S. Vogel, L. Ehm, K. Knorr, G. Braun, Adv. X-ray Anal. 45 (2002) 31.
[20] D. Lovy, Program *SPECTRAW*, Version 1.40, Département de Chimie Physique, University of Geneva, Switzerland, 1996.
[21] J. Rodriguez-Carvajal, Physica B 192 (1993) 55.J. Rodriguez-Carvajal, PROGRAM FullProf.2 k — version 3.20, Laboratoire Léon Brillouin (CEA-CNRS), France, 2005 (The complete program and documentation can be obtained from http://www.ill.eu/sites/fullprof/).
[22] M. François, G. Renaudin, O. Evrard, Acta Cryst. C54 (1998) 1214.
[23] G. Renaudin, F. Kubel, J.-P. Rivera, M. François, Cem. Concr. Res. 29 (1999) 1937.
[24] G. Renaudin, M. François, O. Evrard, Cem. Concr. Res. 29 (1999) 63.
[25] M.S. Crowley, J. Am. Ceram. Soc. 47 (1964) 144.
[26] JCPDS — International Centre for Diffraction Data, PDF2 Data Base, Release 2001, ID 42-0062 for C4ASH14, and ID 83-1289 for C4ASH12.
[27] R. Allmann, Neues Jahrb. Mineral. Monatsh. H3 (1977) 136.
[28] G. Renaudin, M. François, Acta Cryst. C55 (1999) 835.
[29] G. Renaudin, J.-P. Rapin, B. Humbert, M. François, Cem. Concr. Res. 30 (2000) 307.
[30] F. Goetz-Neunhoeffer, J. Neubauer, P. Schwesig, Cem. Concr. Res. 36 (2006) 65.